environments

MDPI

Article

Influence of Rainfall on Urban Non-Point Source Pollution in Rivers from an Event-Based Perspective in Taihu Basin

Ye Pan [1], Qiqi Yuan [2], Jiaxun Guo [3], Haigang Jia [4,*] and Lachun Wang [2]

[1] School of Cruise & Art Design, Jiangsu Maritime Institute, Nanjing 211170, China; 20231138@jmi.edu.cn
[2] School of Geography and Ocean Science, Nanjing University, Nanjing 210023, China
[3] School of Environment and Spatial Informatics, China University of Mining and Technology, Xuzhou 221116, China
[4] Institute of Ecological Civilization and Forestry Development with Chinese Characteristics, Nanjing Forestry University, Nanjing 210037, China
* Correspondence: jhg@njfu.edu.cn; Tel.: +86-025-6822-4709

Abstract

Urban point source pollution has been effectively controlled in recent years; however, rainfall-driven non-point source (NPS) pollution has become a major contributor to the deterioration of urban water environments. This study focuses on the plain river network region of Wuxi City in the Taihu Basin, China. By integrating field monitoring with coupled model simulations, this study upscaled results from the experimental plot to the urban-scale river network, enabling analysis of the full processes of pollutant inflow and transport and evaluation of the role of rainfall in regulating these dynamics. Field monitoring in the experimental plot demonstrated a strong correlation between the temporal dynamics of NPS pollutant inflows and rainfall characteristics. Further analysis using model simulations in the river network area revealed that rainfall, maximum 1 h rainfall, and rainfall duration were identified as the primary drivers of pollutant inflows, while early drought duration, rainfall intensity, and variance between rainfall per unit time exerted non-linear effects. Specifically, when early drought duration was approximately 6–7 days or when rainfall intensity ranged from 2.1 to 2.6 mm/h, riverine nitrogen (N) and phosphorus (P) concentrations and pollutant loadings reached their peaks. In addition, when the deviation of unit-time rainfall from the event mean was between 1.8 and 2 mm, the duration of increase in pollutants entering the river was the longest. This study provides quantitative evidence highlighting the influence of rainfall characteristics on nitrogen and phosphorus dynamics in plain river network urban rivers. The findings offer valuable insights into the remediation of urban black-odor water bodies.

Keywords: urban NPS pollution; pollutant inflow process; rainfall characteristics; plain river network cities

Check for updates

Academic Editor: Daniel D. Gang

Received: 13 January 2026
Revised: 10 February 2026
Accepted: 11 February 2026
Published: 13 February 2026

Copyright: © 2026 by the authors. Licensee MDPI, Basel, Switzerland. This article is an open access article distributed under the terms and conditions of the Creative Commons Attribution (CC BY) license.

1. Introduction

Urbanization exerts a profound influence on the surface water environment [1]. These changes further result in the degradation of urban rivers and adjacent water bodies through point source pollution (e.g., discharges from pipelines) and non-point source (NPS) pollution (e.g., pollutants carried by stormwater runoff) [2,3]. While point source pollution has been effectively controlled in most regions of China, urban NPS pollution has attracted increasing attention [4,5]. The inflow of NPS pollution into rivers has become a major driver of the ecological deterioration of receiving water bodies in urban areas [6]. Consequently,

research on urban NPS pollution and the remediation of black-odor water bodies has become an essential component of improving urban water environments. An effective prerequisite for controlling urban water pollution is to clarify the dominant characteristics of NPS pollution and its inflow and diffusion in rivers, as well as the methodological approaches to study them [7,8].

The process of NPS pollutants entering rivers mainly refers to the accumulation of pollutants during dry weather, followed by their transport into receiving water bodies along the ground surface or drainage pipelines under the scouring effect of stormwater runoff, thereby causing water pollution [9]. In plain river network regions, a typical water environmental problem induced by urban NPS pollution is eutrophication, which threatens both natural ecosystems and drinking water security [10,11]. Urban NPS pollution is characterized by spatiotemporal heterogeneity and diverse transport pathways [12]. From the perspective of temporal variation, the inflow process of urban NPS pollution is strongly affected by rainfall [13], with higher pollutant concentrations during the rainy season [14]. From a spatial perspective, road runoff and roof runoff are important sources of riverine NPS pollution [15,16]. The impact of rainfall on the inflow process of urban NPS pollution is much greater than that of land cover types [17,18]. The magnitude of rainfall events serves as a critical factor affecting this process. Under different rainfall characteristics, the impacts of urban NPS pollution input on river water quality vary [19,20]. Rainfall characteristics are generally quantified as rainfall, rainfall intensity, rainfall duration, antecedent dry days, among others. Although several studies have examined the effects of rainfall characteristics on urban runoff generation and have attempted to rank the relative influence of different rainfall properties on runoff-associated pollutant inflows [21–23], quantitative assessments of how rainfall characteristics regulate the processes of urban NPS pollutants into receiving rivers remain limited, particularly with respect to their direct applicability to specific urban river systems.

To fully understand the characteristics of urban NPS pollution and its diffusion into rivers, current research methods mainly employ field monitoring [24,25], statistical analysis [15], and numerical modeling. Multi-site field monitoring offers the advantage of providing direct evidence for the study of NPS pollution. However, it exhibits considerable limitations in analyzing the large-scale processes of NPS pollution inflow and diffusion [26,27]. Model simulations can compensate for the spatial limitations of field monitoring [28]. Nevertheless, no single model can fully capture the entire diffusion process of NPS pollutants entering rivers [19,29]. Numerous urban NPS pollution models and river water environment simulation models have been developed both domestically and internationally [30,31]. Among them, the Storm Water Management Model (SWMM), as a dynamic rainfall–runoff simulation model, has particular advantages in reproducing complex sewer systems [32–34]. The MIKE model also provides convenient and accurate simulation capabilities for river network environments [35]. At present, many studies have employed coupled models to analyze urban flood risk assessment [36,37] and to optimize NPS pollution control strategies [38,39]. However, studies on input–response models describing the transport of stormwater runoff into receiving water bodies remain relatively limited [20,40,41]. For plain river network urban regions, it is necessary to explore an approach for characterizing the process of NPS pollutants into rivers.

In this study, a plain river network urban region located in the Binhu District and Liangxi District of Wuxi City, China, was selected as the research area. This region is adjacent to Meiliang Bay in the northern part of Taihu Lake, where algal blooms frequently occur [42] and urban black-odor water bodies are also common [43]. By integrating modeling and field monitoring, this study aims to: (1) clarify the inflow, transport, and attenuation processes of NPS pollutants in plain urban river networks; (2) explore the feasibility of

simulating these processes in plain river network cities; and (3) quantitatively investigate the impacts of rainfall characteristics on nitrogen and phosphorus dynamics in plain river networks. This study proposes and applies a network-scale analytical framework that integrates modeling with field observations, seeking to demonstrate its applicability and transferability to similar cities and to extend urban non-point source pollution assessment from individual rivers to whole river network systems. The findings of this study provide a scientific basis for the refined management of urban water environments.

2. Materials and Methods

2.1. Study Area

2.1.1. Location of the Study Area

The study area is located in the junction of the Binhu District and Liangxi District in Wuxi City, China, adjacent to Taihu Lake (Figure 1A). The extent of the study area was delineated based on the layout of the urban drainage system in Wuxi, encompassing the urban area in which surface runoff ultimately drains into two rivers, the Liangxi River and the Ma Ligang River. The northern boundary is defined by the Huishan hill, the southwestern boundary extends to Lihu Lake, and the eastern boundary is close to the Beijing–Hangzhou Canal, with a total area of 27.7 km^2. In addition, the Lucun River, which serves as an important watercourse connecting Lihu Lake and the Beijing–Hangzhou Canal, is also included in the study area. The urban catchment draining into the Lucun River, covering an area of 1.5 km^2, was designated as the experimental plot for model construction (Figure 1B).

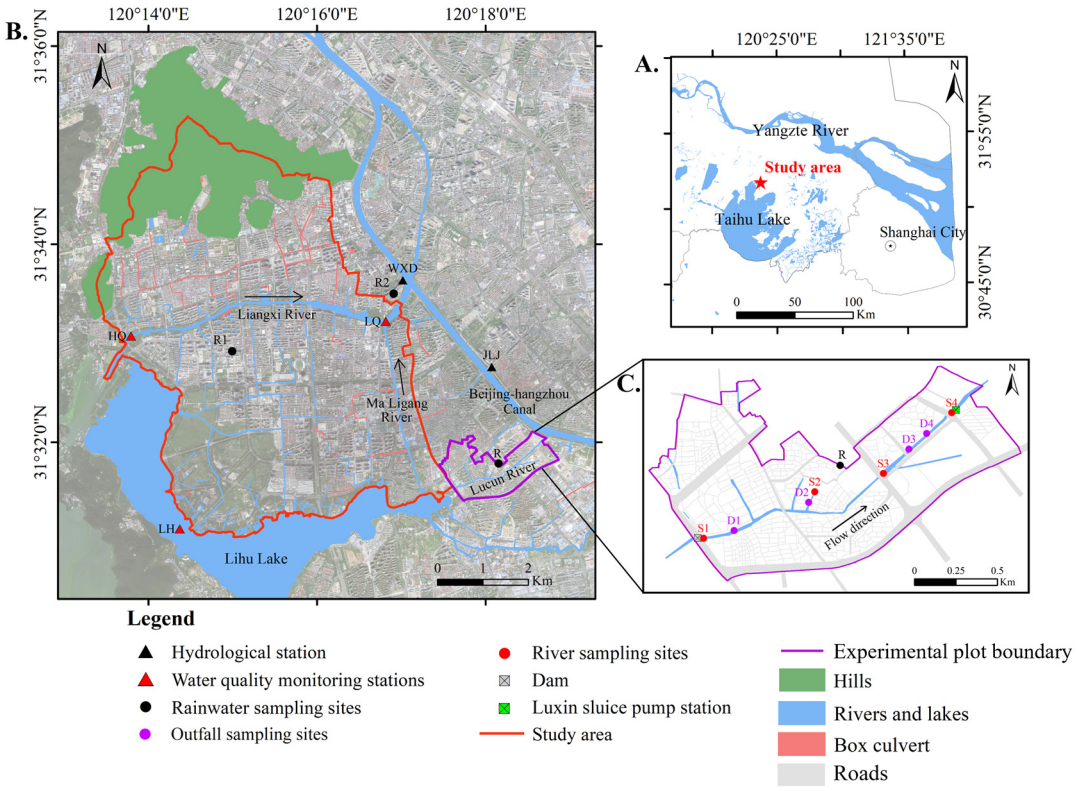


Figure 1. Location of the study area (**A**) and some sampling sites (**B**,**C**).

Both the study area and the experimental plot are situated in a subtropical monsoon climate zone, where cumulative precipitation from May to September accounts for 62% of the annual total. Aside from the hilly terrain in the north, the topography of the study area is relatively flat (Figure S1a). Impervious surfaces constitute 55% of the total area, and the

study area encompasses eight distinct land-use types (Figure S1b). Moreover, the urban drainage system is designed as a separated system for stormwater and wastewater, with stormwater pipelines designed for a 10-year return period (Figure S1c). The river network within the study area is dense, with numerous dead-end channels and box culverts. In total, 52 rivers are distributed across both the experimental plot and the study area, of which 46 are located within the study area. These rivers are hydraulically regulated through sluices and pumping stations (the locations of sluices and pumping stations in both the study area and the experimental plot are shown in Figure S1d). Due to weak hydrological connectivity between rivers, water exchange is extremely limited, resulting in frequent outbreaks of cyanobacterial blooms.

The experimental plot is directly adjacent to the study area, with a comparable level of urban development, similar land-use types, and a relatively consistent degree of stormwater drainage system construction, thereby minimizing environmental heterogeneity. Consequently, the runoff generation and confluence processes can be assumed consistent across both areas. Furthermore, the Lucun River flows from west to east, with clearly defined upstream and downstream sections, both regulated by sluice gates (Figure 1C). As water flow variations can be effectively monitored and water balance validated, the experimental plot can be regarded as highly representative of the hydrological and water quality processes occurring across the broader study area.

2.1.2. Rainfall Characteristics in the Study Area

Two hydrological stations, WXD and JLJ (locations shown in Figure 1), within the study area recorded rainfall from 10 May 2021 to 14 June 2022 in the northern and southern regions of the Liangxi River, respectively. The northern region received 1433.8 mm of rainfall, which was 83.8 mm more than that in the southern region. Monthly rainfall during the analysis period is shown in Figure 2. Combined with the proportion of monthly rainfall to annual rainfall in Wuxi City from 1990 to 2023 (Figure S2), it was found that intra-annual rainfall in the study area is characterized by higher rainfall in spring and summer, and lower rainfall in autumn and winter.

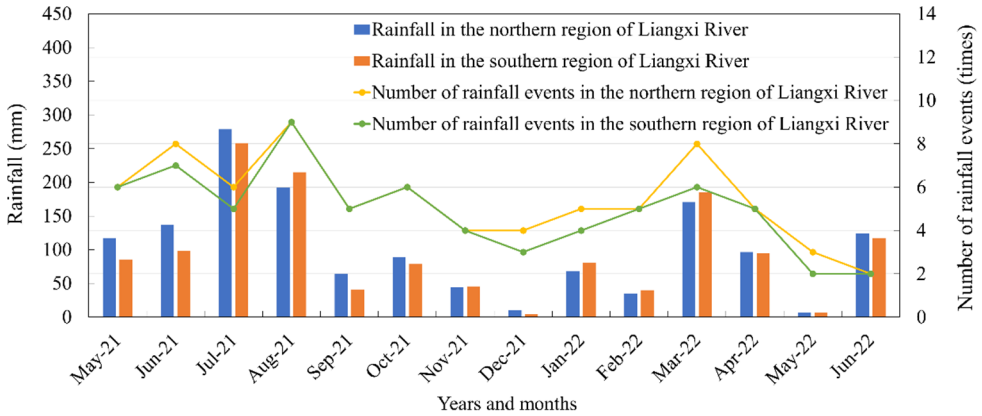


Figure 2. Monthly rainfall and corresponding rainfall event numbers in the areas north and south of Liangxi River from 10 May 2021 to 14 June 2022.

During the study period, 76 rainfall events occurred. The number of rainfall events in the southern region of the Liangxi River was seven fewer than that in the northern region, all of which were classified as light rain. The number of rainfall events per month is shown in Figure 2, with the highest frequency occurring in August 2021 (nine events). Seven rainfall characteristics were calculated for each event. Furthermore, a detailed analysis will be presented in Section 3.3. Four rainfall volume characteristics included total rainfall (mm), rainfall intensity (mm/h), maximum 1 h rainfall (mm), and initial 3 h rainfall (mm).

Three temporal characteristics included rainfall duration (h), early drought duration (h) (i.e., the number of hours without rain before the event), and variance between rainfall per unit time (mm^2), which reflects the rainfall pattern.

2.2. Research Framework

A research framework was established to quantitatively assess the influence of rainfall on NPS pollutants input into rivers within plain river network cities, following three key steps (Figure 3). First, based on the collection of samples and datasets, the characteristics of NPS pollutants input into rivers were investigated within the experimental plot. These investigations were conducted by separately analyzing different types of rainfall events and consecutive rainfall periods. Next, simulation analyses for the plain river network urban area were conducted through a modeling approach. The SWMM and MIKE11 were loosely coupled, and an Urban Non-Point Source Pollution Transport Model (UNSPTM) was first constructed within the experimental plot. Upon validation, the UNSPTM was subsequently extended and applied to the entire study area. Finally, rainfall characteristics within the study area were examined using field-measured data. By integrating the simulation results from the study area, statistical methods such as correlation analysis were employed to explore the influence of rainfall on NPS pollutants input into rivers in plain river network urban environments.

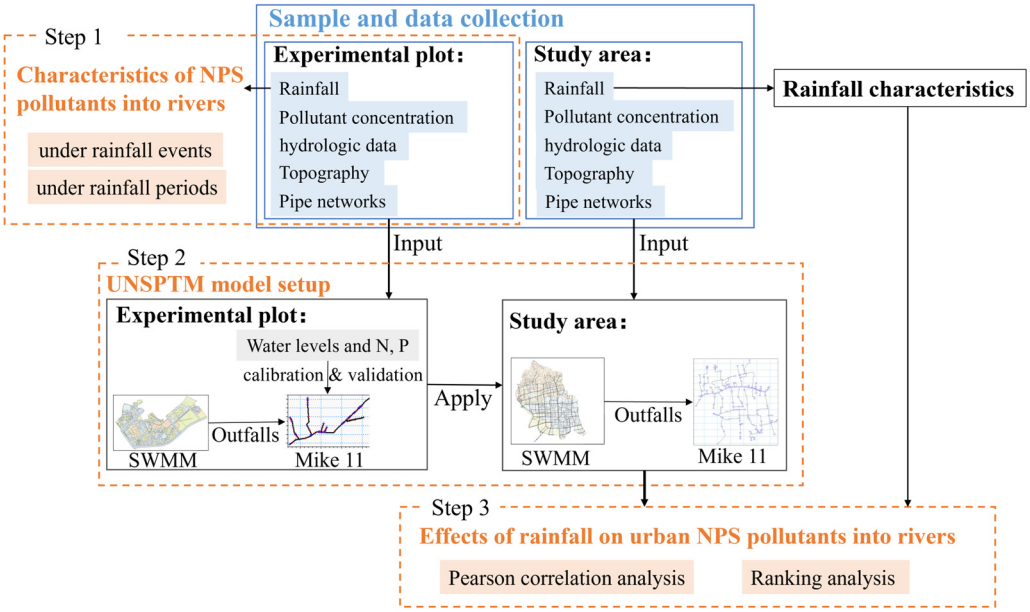


Figure 3. Research framework to assess the impact of rainfall on NPS pollutants into rivers in Taihu Lake Basin urban area.

2.3. Sampling and Analysis in Experimental Plot

The sampling sites within the experimental plot are shown in Figure 1C. Four river sampling points (S1–S4) were established along the Lucun River, with flow direction from S1 to S4. A dam upstream of S1 interrupted the hydrological connection between Lihu Lake and the Lucun River. Downstream of S4, the Luxin sluice-pump station was constructed, controlling the hydrological connectivity between the Lucun River and the Beijing–Hangzhou Canal. In addition, four rainwater outfalls (D1–D4) along the Lucun River were selected as sampling sites.

Between 2021 and 2022, a total of seven sampling campaigns were conducted. At least one rainfall event occurred during each sampling campaign. Detailed rainfall characteristics are presented in Tables 1 and 2. The collected samples and datasets were used to analyze

the characteristics of NPS pollutants input into rivers in plain urban areas, as well as for the calibration and validation of UNSPTM.

Table 1. Rainfall characteristics of the events.

Rainfall Events	Start–End Time	Rainfall (mm)	Rainfall Type	Rainfall Duration (h)	Maximum Rainfall Intensity (mm/h)
Event 1	14 May 2021, 11:00–15 May 2021, 17:00	11.8	Moderate rain	16	7.2
Event 2	10 June 2021, 08:00–12 June 2021, 08:00	0.6	Light rain	2	0.4
Event 3	25 June 2021, 22:00–26 June 2021, 12:00	2.8	Light rain	12	1.2
Event 4	12 June 2022, 10:00–15 June 2022, 00:00	3.6	Light rain	19	1.2
Event 5	23 June 2022, 07:00–26 June 2022, 12:00	77.4	Rainstorm	31	24.8

Table 2. Rainfall characteristics of the two rainfall periods.

Rainfall Periods		Start–End Time	Rainfall (mm)	Rainfall Type	Rainfall Duration (h)	Maximum Rainfall Intensity (mm/h)
Rainfall period 1	Event 6	1 March 2021, 00:00–7 March 2021, 5:00	14	Moderate rain	22	3
	Event 7		1.8	Light rain	6	0.6
	Event 8		1.6	Light rain	7	0.8
Rainfall period 2	Event 9	28 June 2022, 13:00–1 July 2022, 14:00	22	Moderate rain	19	7
	Event 10		3.6	Light rain	1	3.6
	Event 11		35.2	Heavy rain	12	15.2

Each sampling campaign in the experimental plot consisted of three main components: (1) measurement of rainfall and collection of rainwater samples, (2) monitoring of rainwater outfall flow and collection of water samples, and (3) measurement of river water levels and collection of river water samples. First, rainfall and rainwater samples were collected at rainwater sampling site R in the central part of the experimental plot (Figure 1C). Second, after each rainfall event, rainwater outfalls were frequently submerged by river water or intermittently exposed, which hindered sample collection at the outfalls. Whenever exposed, one accessible rainwater outfall among D1, D2, D3, and D4 (Figure 1C), was selected for flow measurement and water sampling. The flow and water quality data from the outfalls were used as input data for the UNSPTM and for sensitivity analysis of model parameters. Finally, for river water level measurements and sampling, ultrasonic depth sounders (SJ-CSW150S, Shandong Shuijing Sensing Technology Co., Ltd.,Weifang, China) were deployed at S1, S2, S3, and S4 (Figure 1C) to measure river depth prior to rainfall events, from which water levels were calculated. River water samples were collected at 30 cm below the water surface in the center of the river using pre-rinsed samplers. After the onset of rainfall, river water levels and samples were collected at S1–S4 at intervals of 0 h, 1 h, 2 h, 4 h, 6 h, 12 h, and 24 h. Among these sites, water level and quality data from S1, S2, and S4 were used as boundary conditions in the UNSPTM, while those from S3 were used for calibration and validation of the UNSPTM.

All water samples were sealed in polyethylene bottles, stored in portable iceboxes, and transported to the laboratory within 24 h of each sampling campaign. Except during events 1, 2, and 3, where ammonium nitrogen (NH_4^+-N) was not analyzed in time, all water samples were analyzed for total nitrogen (TN), total phosphorus (TP), and NH_4^+-N. Unfiltered water samples were used to analyze TN and TP, while filtered samples were used for NH_4^+-N analysis. Water sample analyses were conducted at the Nanjing Institute of Geography and Limnology, Chinese Academy of Sciences, using a continuous flow analyzer (Skalar San plus, Skalar Analytical B.V., Breda, The Netherlands). Detection limits: TN and NH_4^+-N = 0.01 mg/L; TP = 0.001 mg/L.

2.4. Data Sources

The datasets required for the UNSPTM construction included spatial attribute data, hydrometeorological data, and pollutant concentration data.

Spatial attribute data comprised vector boundaries, topography, land use, stormwater drainage system maps, river network morphology, and the operation of sluice-pump stations. Vector boundaries, topography, and land use data for both the experimental plot and the study area were obtained from Google Maps (Google LLC, Mountain View, CA, USA; accessed on 1 January 2021). The stormwater drainage system maps, river network morphology, and operation of sluice-pump stations in the experimental plot and study area were provided by the Binhu District Water Resources Bureau and the Liangxi District Hydrology Bureau of Wuxi City.

Hydrometeorological data included rainfall, flow velocity at rainwater outfalls, and river water levels. Pollutant concentration data included concentrations of TN, TP, and NH_4^+-N in rainwater, rainwater outfalls, and river water. For the experimental plot, hydrometeorological data and pollutant concentration data were collected and recorded in the field. For the study area, hydrometeorological data and pollutant concentration data were collected between 10 May 2021 and 14 June 2022, with separate datasets acquired for the regions north and south of the Liangxi River. The specific data sources are presented in Text S1 in the Supplementary File.

2.5. Model Setup

We integrated the SWMM (v5.2), developed by the U.S. Environmental Protection Agency [44], and the MIKE 11 (v2019), developed by the Danish Hydraulic Institute [35], to construct the UNSPTM. SWMM was employed to build the urban non-point source pollution model, while MIKE 11 was used to establish the river hydrodynamic and water quality model. Subsequently, the two models were coupled to form UNSPTM (Figure 2). Initially, the construction of UNSPTM was carried out within the experimental plot.

2.5.1. Construction of SWMM

SWMM is a dynamic rainfall–runoff simulation model, which is used for planning, analysis, and design related to stormwater runoff and urban drainage systems. This study employed SWMM version 5.1, in which the experimental plots were divided into 534 sub-catchments, the study area was divided into 1050 sub-catchments, and the proportions of greenbelts, roofs, and pavements within each sub-catchment were identified. The stormwater drainage systems of the experimental plot and the study area were conceptualized as networks of pipes, inspection wells, and rainwater outfalls, comprising 359 pipes, 359 inspection wells, and 75 outfalls in the experimental plot, and 1231 pipes, 1213 inspection wells, and 127 outfalls in the study area. We use the Horton model to calculate soil infiltration, due to the fact that the major portion of the catchment is impervious. The dynamic wave method is chosen for simulating flow in pipes. In terms of water quality simulation, we use the saturation function as the surface pollutant build-up algorithm in SWMM. The exponential function is used as the surface pollutant wash-off algorithm. The specific model configuration followed Pan, Guo, Yang et al. [45].

Parameters in SWMM include hydrological parameters, hydraulic parameters, and water quality parameters. Based on the analysis of spatial attribute data for the experimental plot, we determine the drainage area of each sub-catchment, overflow width of each sub-catchment, average surface slope, percentage of impervious area, and geometrical parameters of drainage pipes. In total, 10 hydrological–hydraulic parameters and 13 water quality parameters were configured in SWMM. The parameter ranges were determined by reference to the SWMM manual and previous studies [19]. The 10 hydrological–hydraulic

parameters included: Manning coefficient of pervious area (N-perv), Manning coefficient of impervious area (N-imperv), depression storage of pervious area (Dstore-perv), depression storage of impervious area (Dstore-imperv), percent with no depression storage (Zero-imperv), minimum infiltration rate (Minrate), maximum infiltration rate (Maxrate), infiltration decay coefficient (Decay), drying time in infiltration (Drying time), and Manning coefficient of pipe (Manning-N). The 13 water quality parameters included: maximum accumulation quantity of greenbelt (Maccum-G), half-saturation constant of greenbelt (Hconst-G), wash-off coefficient of greenbelt (Wcoeff-G), wash-off exponent of greenbelt (Wexpo-G), maximum accumulation quantity of pavement (Maccum-P), half-saturation constant of pavement (Hconst-P), wash-off coefficient of pavement (Wcoeff-P), wash-off exponent of pavement (Wexpo-P), removal rate by pavement sweeping (Remrate-P), maximum accumulation quantity of roof (Maccum-R), half-saturation constant of roof (Hconst-R), wash-off coefficient of roof (Wcoeff-R), and wash-off exponent of roof (Wexpo-R).

2.5.2. Construction of MIKE11

MIKE 11 is a hydrodynamic and water quality model for rivers, applicable to pollutant transport and water quality assessments. Using its hydrodynamic and advection–dispersion modules, a one-dimensional model was developed for the Lucun River of the experimental plot, which consists of one main channel and five dead-end river channels, represented by 58 cross-sections. In the study area, a total of 195 cross-sections were delineated across 46 rivers. The initial conditions of the model included both open and closed boundaries. For the experimental plot, the open boundaries were located at sampling sites S1, S2, and S4 (see Figure 1), while all other parts were closed. In the study area, the open boundaries were set as the sluice-pump stations in the Liangxi River, Ma Ligang River, and Lihu Lake (specific locations shown in Figure S1d), while all other boundaries were closed. The open boundaries were assigned water level and water quality time-series data. Additionally, the operational conditions of sluices and pumping stations were incorporated into the model through the hydraulic structures module.

The key parameters of MIKE11 in this study mainly include bed resistance, dispersion coefficient, and decay coefficient. The ranges of these parameters were first identified based on the MIKE 11 User Manual and values reported in previous studies in the Taihu Lake Basin and other similar plain river network systems [29,46,47]. In particular, because MIKE11 solves a one-dimensional advection–dispersion equation, the dispersion coefficient specified in the model is treated as a longitudinal dispersion coefficient. Its magnitude was determined through a combined approach in this study: (i) the expected scale of near-field lateral mixing around the outfall was first assessed using the commonly applied relationship [48] as a reference for order of magnitude; and (ii) a final value was then selected to be consistent with the range of longitudinal dispersion coefficients reported for plain river networks in the Taihu Lake Basin and comparable systems.

2.5.3. Construction of UNSPTM

UNSPTM was established by coupling SWMM and MIKE 11. A loose data coupling approach was adopted, in which the two models remained independent but exchanged simulation results. Specifically (Figure 3), SWMM was first run to obtain outfall discharge and pollutant concentration time series. The spatial positions of the outfalls along the river were then identified, and the discharge and pollutant concentration data were imported as lateral inflows in MIKE11. MIKE 11 was subsequently run to simulate the processes of transport and degradation of urban NPS pollutants within the river.

2.5.4. Method of UNSPTM Performance Evaluation

The performance of UNSPTM was evaluated in detail in Section 3.2, including parameters sensitivity analysis, UNSPTM calibration and validation. Parameter sensitivity analysis, calibration, and validation were conducted using the Parameter Estimation tool [49].

Parameter sensitivity analysis was performed by comparing the weighted sum of squared residuals between observed and simulated values, and calculating the composite scaled sensitivity (CSS) of each parameter. CSS is unitless, and parameters with a CSS value greater than 1 are classified as highly sensitive [50,51]. In this study, sampling results from event 4, event 5, and rainfall period 2 were selected for sensitivity analysis of UNSPTM parameters. The sampling results included outfall flow processes, variations in water quality at outfalls, and variations in water level and water quality in the river.

The prerequisite for accurate simulation of water levels and water quality by UNSPTM is mass balance of water volume. Accordingly, calibration and validation of UNSPTM proceeded in the following steps: First, calibration and validation of river water volume changes were conducted. Next, calibration and validation of the water level process at sampling site S3 of the Lucun River were performed. Finally, calibration and validation of the water quality process at sampling site S3 of the Lucun River were carried out. Observed data from event 3, event 4, and event 5 were used for calibration, while observed data from event 1, event 2, and rainfall period 2 were used for validation. The accuracy of UNSPTM was evaluated using three statistical indicators: Percent Bias (PBIAS), Nash–Sutcliffe efficiency coefficient (NSE), and Root Mean Square Error (RMSE). A good simulation performance was indicated when PBIAS < 25%, NSE > 0.5, and RMSE close to 0 [52,53].

3. Results and Discussion

3.1. Characteristics of Urban NPS Pollutants into River

3.1.1. Characteristics of N and P Concentrations Under Different Types of Rainfall Events

The different types of rainfall events analyzed in this study are event 2, event 1, and event 5, corresponding to light rain (rainfall < 10 mm), moderate rain (10 mm $\leq$ rainfall < 25 mm), and rainstorm (50 mm $\leq$ rainfall < 200 mm), respectively [54]. Detailed rainfall characteristics are shown in Table 1.

Figure 4 shows the temporal variation in N and P concentrations in the Lucun River during events 2, 1, and 5. It can be observed that, regardless of rainfall magnitude, river water quality generally increased following rainfall onset, followed by a gradual leveling off or even a decline once rainfall ceased. During event 2, the river mean TN increased from 4.15 mg/L to 8.66 mg/L before declining to 5.26 mg/L, while TP rose from 0.333 mg/L to 0.737 mg/L before decreasing to 0.369 mg/L. In event 1, TN increased from 9.52 mg/L to 13.35 mg/L before declining to 9.23 mg/L, while TP rose from 0.535 mg/L to 1.059 mg/L before decreasing to 0.526 mg/L. In event 5, TN increased from 4.06 mg/L to 12.43 mg/L before declining to 8.72 mg/L, while TP rose from 0.188 mg/L to 0.914 mg/L before decreasing to 0.585 mg/L.

The experimental plot employed a separated sewer system; therefore, during rainfall events, the majority of pollutants entering the Lucun River originated from rainfall itself and from the wash-off of accumulated pollutants on urban surfaces and within the drainage system [55,56]. Thus, NPS pollutants entering rivers typically exhibited a clear pattern: rapid increase after rainfall peak, followed by gradual decline once rainfall ceases. Similar findings have been reported previously. For instance, a field survey in urban rivers of Beijing revealed that TN, TP, and NH_4^+-N all increased sharply after rainfall and subsequently decreased [57]. Moreover, model-based studies have shown that the peak pollutant concentrations in receiving rivers generally occur approximately three hours after rainfall, lasting for about one hour, before returning to pre-event levels roughly seven hours later [58]. In

the present study, the temporal patterns of N and P concentrations were similar across the three rainfall events, whereas their magnitudes differed. Peak concentration increases were greatest during the rainstorm event, followed by the moderate rainfall event, and were lowest during the light rainfall event. This indicates that increasing rainfall volume and intensity progressively enhance the contribution of urban NPS pollutants to rivers, consistent with related studies [6]. Specifically, in event 2 (light rain), TN and TP increased by 109% and 121%, respectively. During event 1 (moderate rain), TN increased by 136% and TP by 319%. During event 5 (rainstorm), TN increased by 206% and TP by 387%.

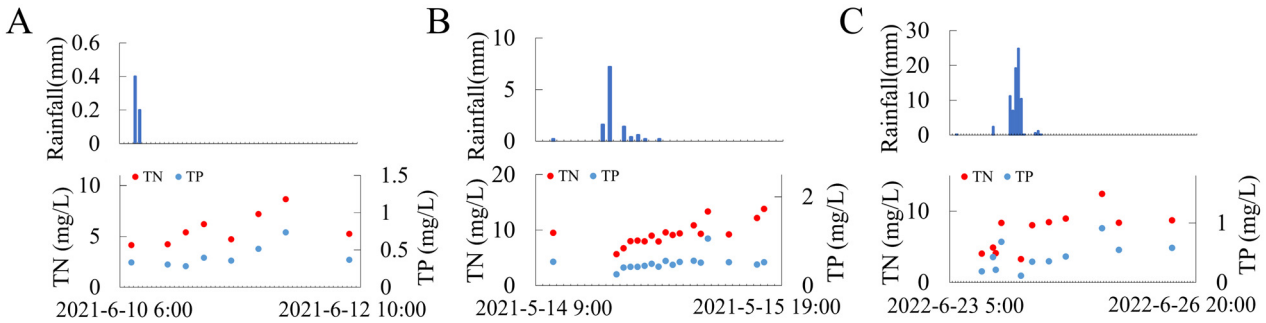


Figure 4. Change process of mean river water quality in event 2 (**A**), event 1 (**B**), and event 5 (**C**).

In addition, the operational scheduling of sluice-pump stations also exerted an influence on the transport of urban NPS pollutants into rivers. Previous studies have demonstrated that enhancing hydrological connectivity in plain river network regions can effectively improve water quality, as increased connectivity promotes the decline of TN and TP at varying rates [59]. However, during rainfall events, i.e., when NPS pollutants are entering rivers, the operation of sluice-pump stations alters hydrological connectivity, thereby affecting the degradation and migration of pollutants [60]. In the experimental plot of this study, the operation of the Luxin sluice-pump station not only served flood-control purposes but also shortened the residence time of NPS pollutants in the river, facilitating their downstream transfer. For instance, during event 5, following the rainfall peak (24.8 mm within one hour), the sluice was closed and the pumps were activated, discharging water into the Beijing–Hangzhou Canal for 4.5 h, with a total outflow volume of 40,050 m^3. A similar operational strategy was applied during event 1, during which the Luxin sluice-pump station discharged water downstream for 1 h, resulting in a total outflow of 5400 m^3. During these processes, the water level upstream of the station declined, and mean river pollutant concentrations also decreased compared with pre-pumping levels, indicating that urban NPS pollutants entering the Lucun River had been transferred downstream to the Grand Canal.

3.1.2. Characteristics of N and P Concentrations Under Different Continuous Rainfall Events

Two continuous rainfall periods (rainfall period 1 and 2) were selected to analyze the characteristics of urban NPS pollutants input into the Lucun River. Each rainfall period contained three rainfall events (two rainfall events were separated by at least a 6 h no-rainfall interval [61]). Detailed rainfall characteristics are summarized in Table 2.

Figure 5 shows the mean variation processes of N and P concentrations in the Lucun River during the two continuous rainfall periods. It can be seen that, during continuous light-to-moderate rainfall events (Figure 5A), river N and P concentrations exhibited an overall gradual increase; whereas during a sequence of heavy rainfall followed by light rainfall (Figure 5B), river N and P concentrations rose sharply after the heavy rainfall and then fluctuated slightly thereafter. In rainfall period 1, mean TN increased from 10.54 mg/L

to 13.44 mg/L, NH_4^+-N from 7.13 mg/L to 10.98 mg/L, and TP from 0.333 mg/L to 1.102 mg/L. In rainfall period 2, the first event raised TN from 12.76 mg/L to 15.20 mg/L, NH_4^+-N from 11.45 mg/L to 14.64 mg/L, and TP from 1.103 mg/L to 1.373 mg/L, whereas subsequent events produced only minor increases.

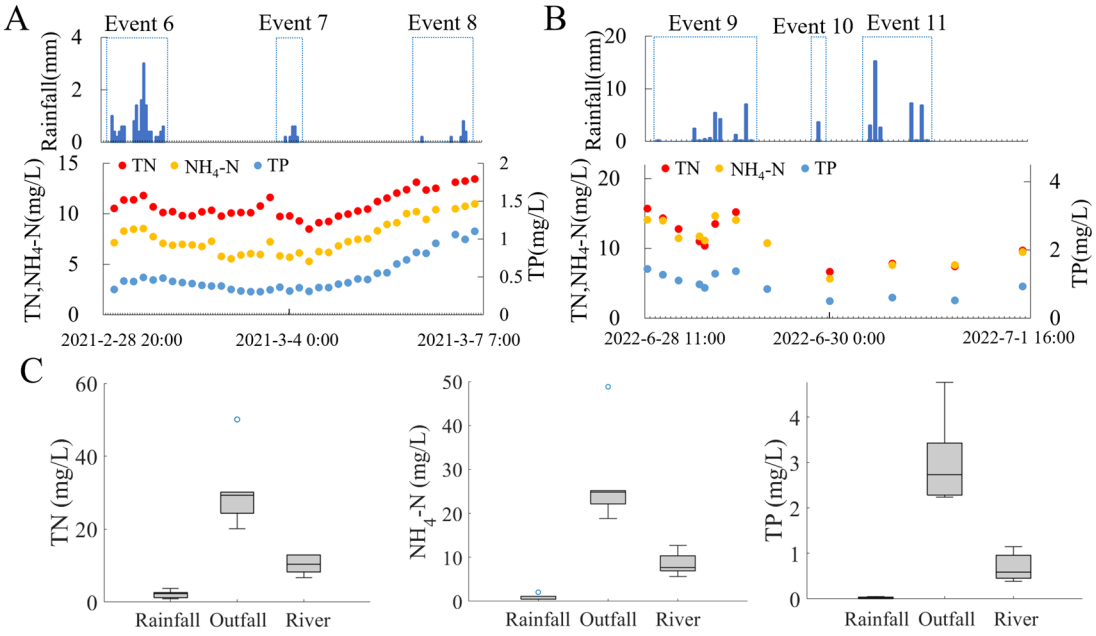


Figure 5. Change process of mean river water quality in rainfall period 1 (**A**) and rainfall period 2 (**B**) and the mean concentration of TN, TP and NH_4^+-N in the rainwater flow path during the two rainfall periods (**C**). In panel (**C**), the box represents the interquartile range, the central line indicates the median, and individual circular points denote outliers beyond the whiskers.

These findings suggest that, in continuous rainfall events of low magnitude, urban NPS pollutants into rivers occurs gradually, as repeated small rainfall events progressively wash pollutants into the river. By contrast, in continuous rainfall events of large magnitude, the process is markedly different: heavy rainfall rapidly flushes the majority of accumulated surface pollutants into the river, leading to sharp nutrient increases. Subsequent rainfall events then mobilize relatively fewer pollutants, resulting in slower concentration rises. Thus, the dynamics of pollutant input during continuous rainfall are influenced by rainfall intensity, pollutant accumulation, and release rates. Previous studies have reported similar behavior. For example, during low-intensity rainfall events with a 1-year return period, surface pollutants are progressively washed into rivers, causing sustained increases in river pollutant concentrations. Low flow conditions further promote pollutant retention and mixing, eventually driving concentrations to peak levels [62]. This explains the steady increases observed in rainfall period 1. By contrast, the sharp rise in nutrients following the first moderate rainfall of rainfall period 2 highlights the stronger first flush effect induced by higher rainfall intensity [63,64]. During the six rainfall events across both periods, mean TN, TP, and NH_4^+-N concentrations in the Lucun River all increased to varying degrees, showing consistent trends.

Marked spatial differences in N and P concentrations were observed along rainwater flow paths. During the six rainfall events of rainfall periods 1 and 2, the N and P concentrations at rainwater outfalls were the highest, being 2–6 times greater than those in the river (Figure 5C). This indicates that rainfall-driven NPS pollution substantially elevate riverine N and P concentrations, exacerbating eutrophication, consistent with previous reports [65,66]. Moreover, NH_4^+-N was the dominant component of TN in both

the stormwater drainage system and the river, with mean NH_4^+-N/TN ratios of 89.2% at drainage outfalls and 83.2% in the river.

3.2. Evaluation of UNSPTM Performance

3.2.1. UNSPTM Parameters Sensitivity Analysis

The UNSPTM constructed in this study is formed by coupling SWMM and MIKE 11, with the model uncertainty primarily arising from parameter uncertainty [67,68]. The UNSPTM contains 26 parameters in total, among which the sensitivity analysis results of 10 hydrologic–hydraulic parameters and 13 water quality parameters are shown in Figure 6. Highly sensitive parameters will become the focus of adjustment during model calibration and verification.

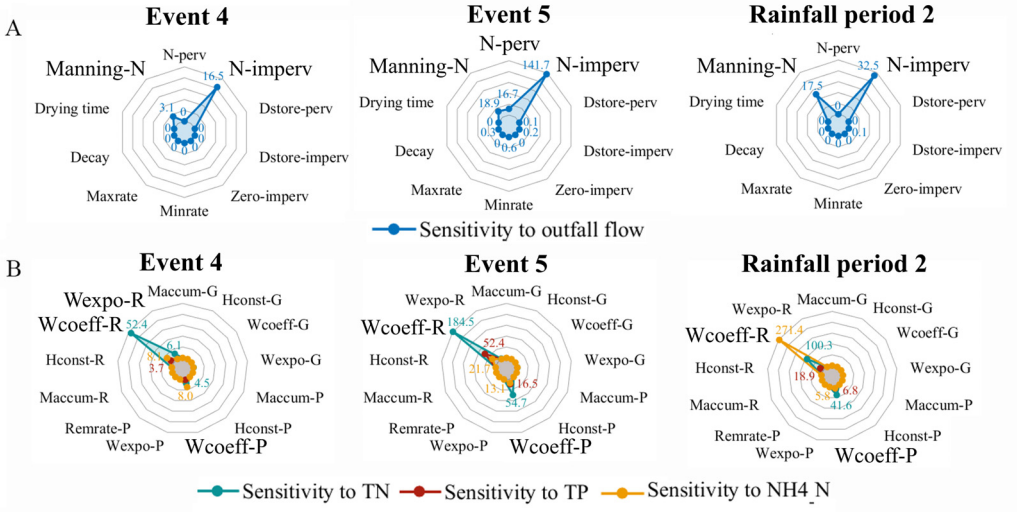


Figure 6. Sensitivity of UNSPTM parameters. (**A**) Sensitivity of hydrological and hydraulic parameters to outfall flow; (**B**) Sensitivity of water quality parameters to water quality.

Figure 6A presents the sensitivity analysis of 10 hydrological–hydraulic parameters with respect to the outfall flow process. Among the hydrologic–hydraulic parameters in the UNSPTM, N-imperv, N-perv, and Manning-N are identified as highly sensitive parameters, as their CSS values are significantly greater than 1. During the three rainfall events of event 4, event 5, and rainfall period 2, CSS values of N-imperv and Manning-N were far greater than 1. Under event 5, the CSS value of N-perv was much greater than 1. These findings are consistent with previous studies, which have reported N-imperv and Manning-N as highly sensitive parameters within the hydrologic–hydraulic parameters of SWMM [69,70].

Figure 6B shows the sensitivity analysis results of 13 water quality parameters with respect to the variation processes of N and P concentrations at the outfall. Among the water quality parameters in the UNSPTM, Wcoeff-R, Wcoeff-P, and Wexpo-R are identified as highly sensitive parameters, as their CSS values are significantly greater than 1. Under event 4, the parameters with CSS values greater than 1 are Wcoeff-P, Wcoeff-R, and Wexpo-R. Under event 5 and rainfall period 2, the parameters with CSS values greater than 1 are Wcoeff-P and Wcoeff-R. CSS values of the other water quality parameters are shown in Tables S1–S3 in the Supplementary File. Meanwhile, some studies have indicated that in SWMM, the maximum accumulation quantity, wash-off coefficient, and wash-off exponent of pavement and roof generally become highly sensitive parameters [70].

MIKE 11 contains one hydraulic parameter and two water quality parameters, among which the dispersion coefficient is a range value, and studies have found that the bed resistance and decay coefficient in MIKE 11 are sensitive parameters [19]. Therefore, this

study conducted sensitivity analysis on bed resistance and decay coefficient. Under event 4, CSS values of bed resistance, TN decay coefficient, TP decay coefficient, and NH_4^+-N decay coefficient were 0.1, 0.6, 0.2, and 0.5, respectively. Under event 5, the corresponding CSS values were 0.4, 0.8, 0.6, and 0.8. Under rainfall period 2, the corresponding CSS values were 0.2, 0.7, 0.5, and 0.7. Therefore, it can be concluded that the sensitive parameters in MIKE 11 are bed resistance and decay coefficient.

3.2.2. UNSPTM Calibration and Validation

In the experimental plot, the calibration results of river water volume changes are shown in Figure 7. During the sampling periods, the simulated river water volume change was obtained by subtracting sluice-pump station discharge from the simulated outflow at rainwater outfalls, while the observed river water volume change was derived from measured water level differences.

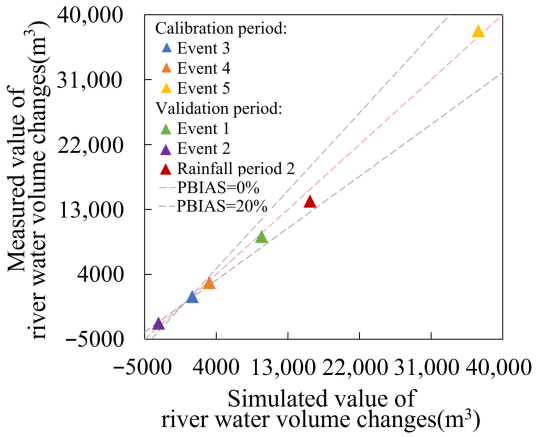


Figure 7. PBIAS of river water volume changes during model calibration and validation period.

During event 3, event 4, and event 5, the PBIAS of water volume changes in the Lucun River was 6.1%, 8.5%, and −2.3%, respectively, with small errors that meet the requirements of simulation. During the three rainfall events in the calibration period, the sluice-pump stations in the Lucun River were operated. In event 3, the Luxin sluice-pump station was opened for 15 min, discharging a total volume of 900 m^3. In event 4, a temporary pump station was installed upstream of the Lucun River and discharged 226 m^3 into the river. In event 5, an upstream pump station discharged 2128 m^3 into the Lucun River. The gate of the Luxin sluice-pump station was opened for 57 h, generating a gate discharge of 9917 m^3. When the gate was closed, the pump station was activated, discharging a total volume of 40,050 m^3.

In the experimental plot, the validation results of river water volume changes are also shown in Figure 7. During event 1, event 2, and rainfall period 2, the PBIAS of river water volume changes was 4.8%, 17.5%, and 11.5%, respectively, all less than 20% [71], meeting the requirements of simulation. During the rainfall events in the validation period, the Luxin sluice-pump station also operated. In event 1, the pump station was opened for 20 min, discharging 1200 m^3. In event 2, the pump station was opened for 55 min, discharging 3300 m^3. During rainfall period 2, the gate was opened for 6 h 45 min, producing a gate discharge of 32,274 m^3. When the gate was closed, the pump station operated for 2 h 15 min, discharging 16,200 m^3.

In the experimental plot, the calibration results of water level variations at point S3 of the Lucun River are shown in Figure 8A. PBIAS during the calibration period ranged from 0.3% to 3.3%, with an absolute error between simulated and observed water levels ranging from 0.01 m to 0.36 m. NSE values were all greater than 0.7, and RMSE values were

close to 0, indicating good calibration performance of UNSPTM for water level processes. Furthermore, as shown in Figure 8A, the simulated and observed processes of river water level fitted well, except during event 5 when the simulated peak water level was higher than the observed value, but the overall trend was accurately reproduced.

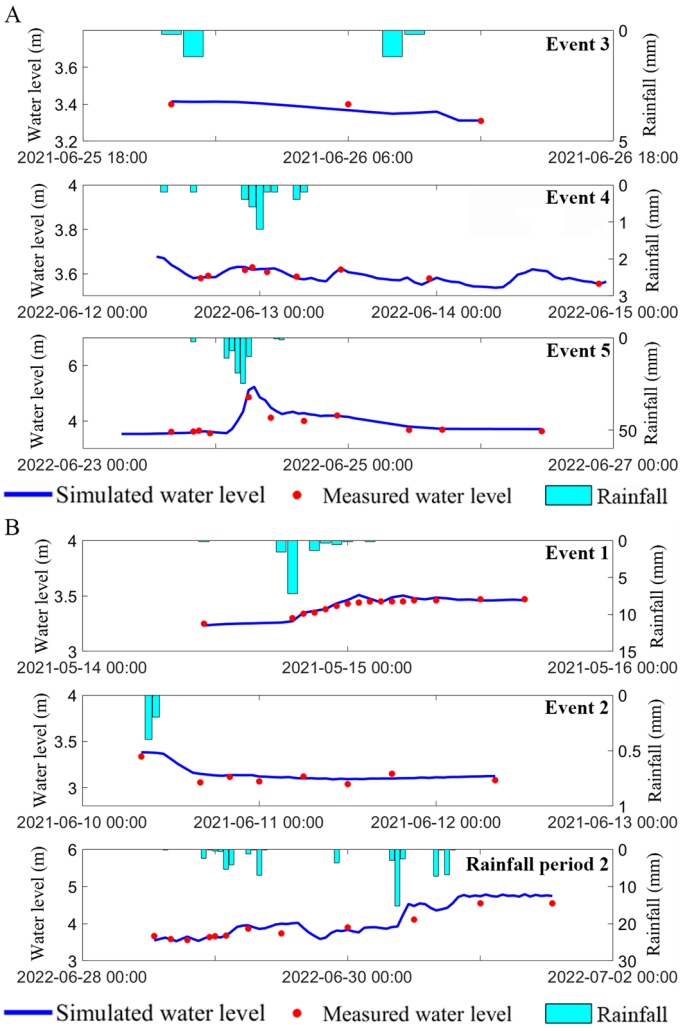


Figure 8. Comparison between measured and simulated water levels at S3 during the calibration period (**A**) and validation period (**B**).

In the experimental plot, the validation results of water level variations at point S3 are shown in Figure 8B. The UNSPTM simulations exhibited strong agreement with observations, with average PBIAS ranging from 0.7% to 3%, absolute errors between 0.01 m and 0.36 m, NSE values all greater than 0.65, and RMSE values close to 0.

Based on the good calibration and validation results of river water volume changes and water level processes, the calibration of TN, TP, and NH_4^+-N concentration processes at point S3 of the Lucun River was carried out, and the results are shown in Figure 9. During the calibration period, the average PBIAS of river water quality was 21.6%. Except for NH_4^+-N in event 5, where the average PBIAS was 40.37%, the PBIAS of other water quality parameters was below 30%. From the NSE results, the average NSE of water quality was 0.54. Except for event 4 where NSE values were generally low, the NSE values of other events were greater than 0.5. From the RMSE results, in event 3 and event 5, the RMSE values were close to 0.

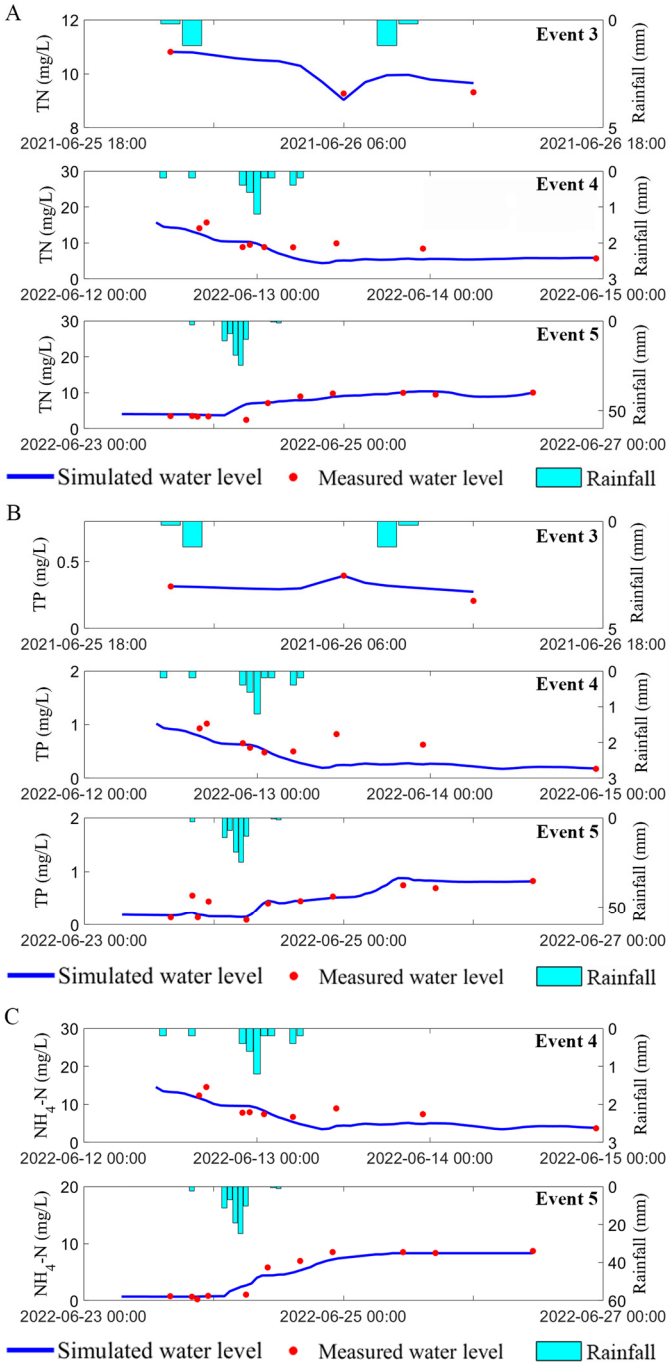


Figure 9. Comparison between measured and simulated TN (**A**), TP (**B**) and NH_4^+-N (**C**) at S3 during the calibration period.

During the calibration period for river water quality processes, the simulation results showed that UNSPTM performed well in reproducing the increases in river water quality after rainfall (Figure 9). However, in event 4, the simulated post-rainfall concentrations were lower than the observed values, which may be related to untreated domestic sewage discharge. During event 4, occasional domestic sewage discharge was observed at drainage outfall D2 in the midstream of the Lucun River. Nevertheless, in the simulation of event 4, the Kling–Gupta efficiency coefficients of TN, TP, and NH_4^+-N concentration processes were 0.68, 0.53, and 0.71, respectively, all greater than 0.5 [72]. Therefore, regarding the variation trends of river N and P concentrations during rainfall events, UNSPTM can basically meet the requirements for water quality simulation.

Figure 10 presents the validation results of TN, TP, and NH_4^+-N concentration processes at point S3 in the Lucun River. During the validation period, the average PBIAS of river water quality did not exceed 25%, the average NSE was 0.67, and RMSE values were close to 0, indicating better performance than in the calibration period. From the NSE results, except for TN in rainfall period 2 with an NSE of 0.28, all other NSE values were greater than 0.5.

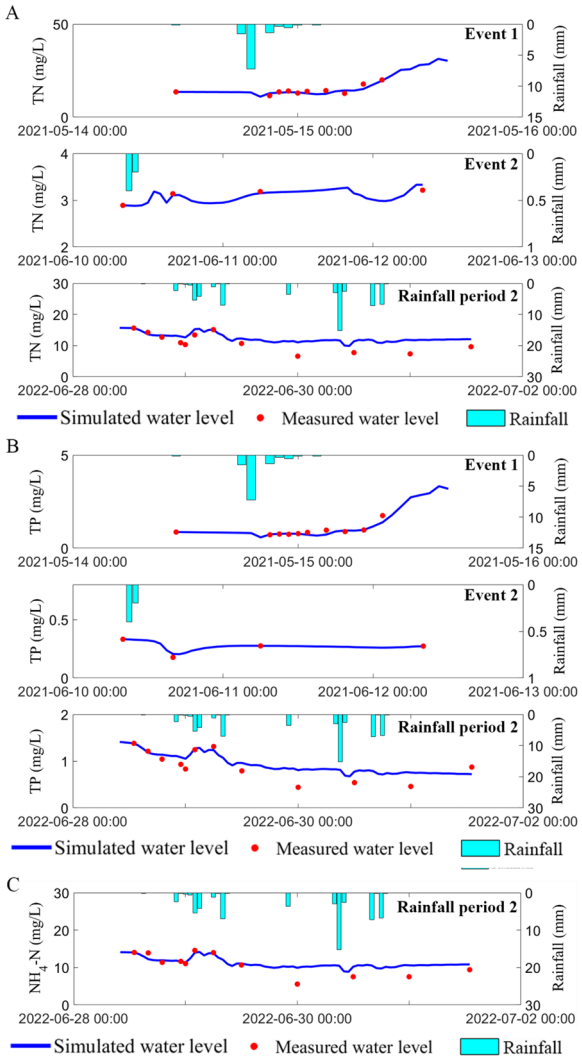


Figure 10. Comparison between measured and simulated TN (**A**), TP (**B**) and NH_4^+-N (**C**) at S3 during the validation period.

During the validation period, the simulation results of water quality processes showed overall agreement with the observed trends (Figure 10). However, in rainfall period 2, the simulated post-rainfall concentrations were higher than the observed values, possibly due to model settings. In SWMM, residual pollutants in the rainwater drainage system are simulated as baseflow, which may not accurately reflect reality, leading to discrepancies between simulated and observed values. Nevertheless, considering the overall process of river water quality variation and PBIAS results, UNSPTM can adequately simulate TN, TP, and NH_4^+-N concentration processes.

Finally, the UNSPTM was established in the study area through a loose coupling approach. The parameter values of UNSPTM in the study area were determined with reference to those obtained in the experimental plot, and the final values of the 26 model parameters are presented in Tables S4–S6 in the Supplementary File.

3.3. Effects of Rainfall on Urban NPS Pollutants Entering Rivers Within Plain River Networks

During the study period (10 May 2021–14 June 2022), UNSPTM was used to simulate the three pollution characteristics, namely pollutants' peak, pollutants' loadings, and pollutants' growth duration in the rivers. Using TN as an example, Pearson's correlation coefficients were calculated between the seven rainfall characteristics and the three pollution characteristics. The results are shown in Figure 11. Similar patterns were observed for TP and NH_4^+-N.

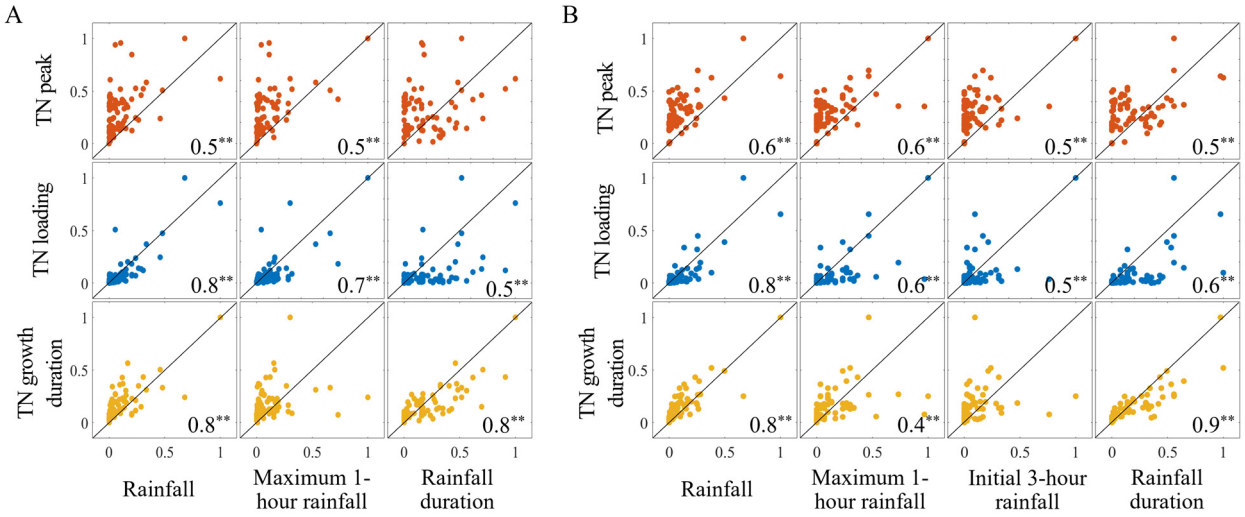


Figure 11. Correlation between the characteristic values of rainfall and TN entering the river in the northern region of the Liangxi River (**A**) and the southern region of the Liangxi River (**B**). The black numbers are the values of the correlation coefficients. '**' represents that the correlation is significant ($p < 0.01$).

The correlation results indicate that rainfall and maximum 1 h rainfall are the main factors influencing pollutants' peak concentrations in rivers within plain river networks. Rainfall, maximum 1 h rainfall, and rainfall duration are the dominant factors affecting pollutants' loadings. Rainfall duration and rainfall were the main factors influencing pollutants growth duration. In addition, in the southern region of the Liangxi River, initial 3 h rainfall also significantly affected pollutants' peak concentrations and pollutants' loadings.

Among the seven rainfall characteristics, rainfall, maximum 1 h rainfall, rainfall duration, and initial 3 h rainfall exerted the strongest influence on the processes of urban NPS pollutants entering rivers within plain river networks. In contrast, the UNSPTM simulation results indicated that early drought duration, variance between rainfall per unit time, and rainfall intensity exhibited non-linear effects on pollutant inflows. Therefore, rainfall events were ranked according to the magnitude of rainfall characteristics, and three corresponding pollution characteristics were analyzed separately for the northern and southern regions of the Liangxi River. For each rainfall event, the pollution characteristics were calculated as the mean values across all rivers within the study area, with averages computed separately for rivers located north and south of the Liangxi River.

The relationship between early drought duration and pollution characteristics is shown in Figure 12. When early drought lasted 155–177 h (approximately 6–7 days), the peak and loadings of N and P were the highest. Previous studies have shown that dry periods lead to the accumulation of surface pollutants and sewer sediments. Pollution accumulation typically peaks after approximately five consecutive dry days [73], consistent with the findings of this study. In the northern region of the Liangxi River, TN peaks and loadings were highest when drought lasted 154–182 h; TP peaks and loadings were highest at 140–177 h; and NH_4^+-N peaks and loadings were highest at 170–182 h. In the southern

region, TN, TP, and NH_4^+-N peaks and loadings were all highest when drought lasted 155–195 h.

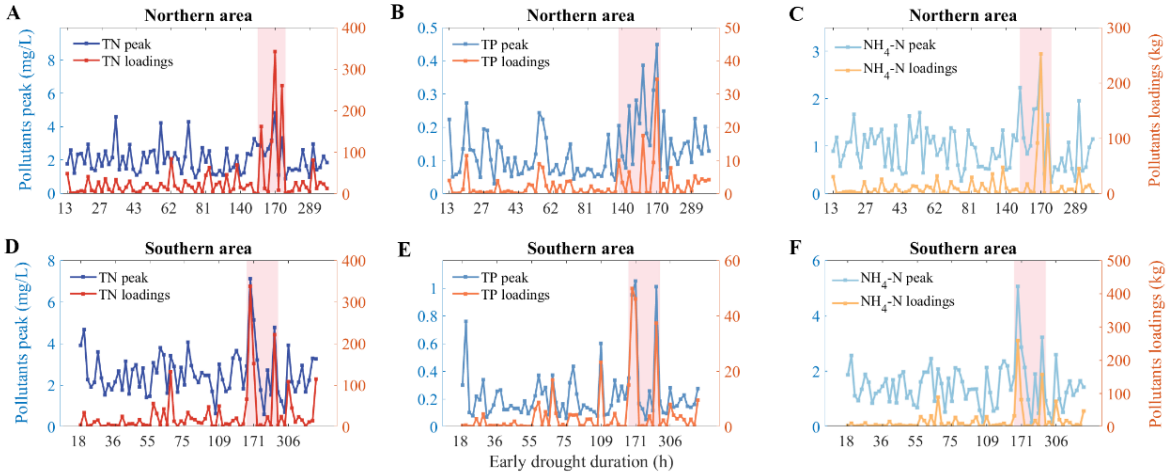


Figure 12. Relationship between early drought duration and pollutants' peak and pollutants' loadings. (**A**–**C**) Area north of the Liangxi River: (**A**) TN; (**B**) TP; (**C**) NH_4^+-N. (**D**–**F**) Area south of the Liangxi River: (**D**) TN; (**E**) TP; (**F**) NH_4^+-N. Pink shaded areas indicate the interval ranges corresponding to the highest values.

The relationship between rainfall intensity and pollution characteristics is shown in Figure 13. When rainfall intensity was 2.1–2.6 mm/h, the peak and loadings of N and P reached their maximum. In the northern region of the Liangxi River, TN peaks and loadings were highest when rainfall intensity was 1.3–2.6 mm/h, while TP and NH_4^+-N peaks and loadings were highest at 1.4–2.6 mm/h. In the southern region, TN peaks and loadings were highest at 2–2.7 mm/h; TP peaks and loadings were highest at both 0.9–1.0 mm/h and 2–2.7 mm/h; and NH_4^+-N peaks and loadings were highest at 2.1–2.7 mm/h.

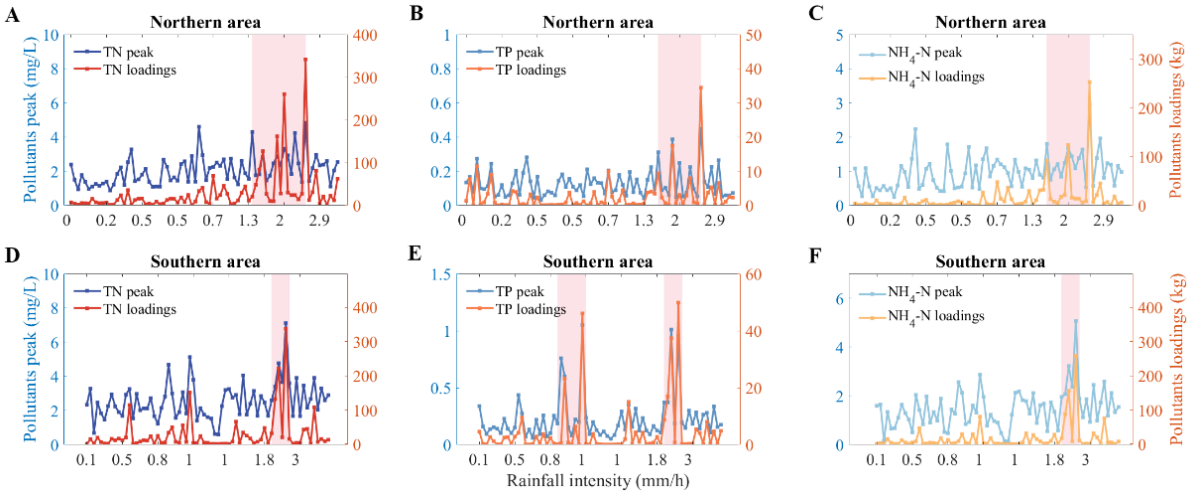


Figure 13. Relationship between rainfall intensity and pollutants' peak and pollutants' loadings. (**A**–**C**) Area north of the Liangxi River: (**A**) TN; (**B**) TP; (**C**) NH_4^+-N. (**D**–**F**) Area south of the Liangxi River: (**D**) TN; (**E**) TP; (**F**) NH_4^+-N. Pink shaded areas indicate the interval ranges corresponding to the highest values.

The relationship between variance between rainfall per unit time and pollutants growth duration is shown in Figure 14. When variance between rainfall per unit time was 3.1–3.9 mm^2, pollutants' growth duration was the longest. In other words, when the deviation of unit-time rainfall from the mean was approximately 1.8–2.0 mm, the

pollutants' growth duration was the longest. In the northern region of the Liangxi River, TN growth duration was longest when variance was 2.5–5.5 mm^2; TP when variance was 2–3.9 mm^2; and NH_4^+-N when variance was 3.1–5.5 mm^2. In the southern region, TN growth duration was longest at 3.1–5.9 mm^2; TP at 0.3–0.7 mm^2 and 3.1–6.0 mm^2; and NH_4^+-N at 3.1–6.0 mm^2.

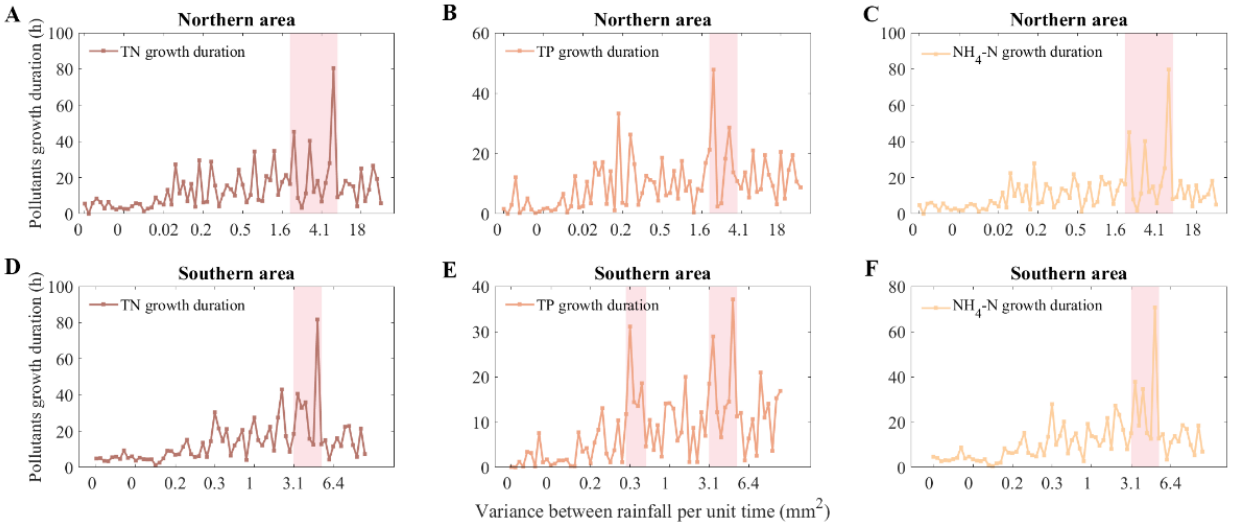


Figure 14. Relationship between variance between rainfall per unit time and pollutants' growth duration. (**A**–**C**) Area north of the Liangxi River: (**A**) TN; (**B**) TP; (**C**) NH_4^+-N. (**D**–**F**) Area south of the Liangxi River: (**D**) TN; (**E**) TP; (**F**) NH_4^+-N. Pink shaded areas indicate the interval ranges corresponding to the highest values.

3.4. Uncertainties and Limitations

Currently, our study has certain limitations. Although we successfully identified the characteristics of NPS pollutants entering rivers in plain urban areas, the scope was limited to seven sampling campaigns and one year of monitoring data, with findings largely derived from model simulations. While the performance evaluation of UNSPTM was satisfactory, uncertainties in the model still remain. Although the natural environment, urban infrastructure, and hydrological management of the experimental plot and the study area are consistent, extrapolation from the experimental plot to the plain urban river network inevitably introduces uncertainties and errors. In real-world conditions, there exists heterogeneity among different sub-catchments, such as vegetation composition, micro-topography, building structures, and paving materials [74]. These differences influence the rainfall–runoff processes of urban sub-catchments, while model limitations also contribute to discrepancies between simulated and actual results. Long-term monitoring or intensive sampling campaigns can effectively complement numerical studies, but they are costly and labor-intensive. Despite these limitations, the numerical simulations presented in this study represent an important step toward better understanding the processes of NPS pollutants entering rivers in plain urban river networks, and they lay a foundation for establishing long-term monitoring networks.

4. Conclusions

Through field monitoring and sampling, the construction of the UNSPTM, and consideration of flood control operation schemes, this study extended the analysis from the experimental plot to the urban river network of the plain area, and comprehensively examined rainfall–runoff processes and the impacts of rainfall on NPS pollutants entering rivers. The results demonstrated that the temporal dynamics of urban NPS pollution inputs are

strongly correlated with rainfall characteristics. At the event scale, pollutant inflows accelerated after the rainfall peak, slowed down following the cessation of rainfall, and ended once rainwater inflow ceased. UNSPTM simulations further revealed that rainfall, maximum 1 h rainfall, and rainfall duration are the dominant factors affecting pollutant inflows in plain urban river networks, whereas early drought duration, rainfall intensity, and variance between rainfall per unit time had non-linear impacts. Specifically, when early drought duration was approximately 6–7 days or when rainfall intensity was 2.1–2.6 mm/h, the peak and loadings of N and P are the highest. When the rainfall depth during a rainfall event deviates from the mean by 1.8–2 mm, the pollutant growth duration was the longest. This study quantitatively highlights the influence of rainfall on N and P dynamics within plain urban river networks, and provides scientific guidance for improving the management of black-odor water bodies in such regions. Moreover, this study demonstrates a degree of applicability and transferability in addressing water environment issues in plain river network cities. By applying the technical framework proposed herein, analyses of urban NPS pollution can be extended beyond individual rivers to encompass entire river network systems, enabling the assessment of rainfall-driven impacts on network-scale water quality.

Supplementary Materials: The following supporting information can be downloaded at: https://www.mdpi.com/article/10.3390/environments13020104/s1.

Author Contributions: Conceptualization, Y.P.; methodology, Y.P., J.G. and L.W.; software, Y.P.; investigation, Q.Y., Y.P. and H.J.; data curation, H.J.; writing—original draft preparation, Y.P.; writing—review and editing, J.G. and L.W.; supervision, L.W.; funding acquisition, L.W. All authors have read and agreed to the published version of the manuscript.

Funding: This research was funded by the Major Science and Technology Program for Water Pollution Control and Treatment (Grant No. 2017ZX07203002-01) and the Doctoral Research Start-up Fund Project of Jiangsu Maritime Institute (Grant No. 2024BSKY09).

Data Availability Statement: Data will be made available on request.

Acknowledgments: The authors would like to acknowledge Jun Zhao, Xueying Huang, and Qihang Hu for their assistance in field studies as well as Chunhua Hu for laboratory analysis.

Conflicts of Interest: The authors declare no conflicts of interest.

Abbreviations

The following abbreviations are used in this manuscript:

NPS	Non-point source
N	Nitrogen
P	Phosphorus
SWMM	Storm Water Management Model
UNSPTM	Urban Non-Point Source Pollution Transport Model
NH_4^+-N	Ammonium nitrogen
TN	Total nitrogen
TP	Total phosphorus
N-perv	Manning coefficient of pervious area
N-imperv	Manning coefficient of impervious area
Dstore-perv	Depression storage of pervious area
Dstore-imperv	Depression storage of impervious area
Zero-imperv	Percent with no depression storage
Minrate	Minimum infiltration rate
Maxrate	Maximum infiltration rate
Decay	Infiltration decay coefficient

Drying time	Drying time in infiltration
Manning-N	Manning coefficient of pipe
Maccum-G	Maximum accumulation quantity of greenbelt
Hconst-G	Half-saturation constant of greenbelt
Wcoeff-G	Wash-off coefficient of greenbelt
Wexpo-G	Wash-off exponent of greenbelt
Maccum-P	Maximum accumulation quantity of pavement
Hconst-P	Half-saturation constant of pavement
Wcoeff-P	Wash-off coefficient of pavement
Wexpo-P	Wash-off exponent of pavement
Remrate-P	Removal rate by pavement sweeping
Maccum-R	Maximum accumulation quantity of roof
Hconst-R	Half-saturation constant of roof
Wcoeff-R	Wash-off coefficient of roof
Wexpo-R	Wash-off exponent of roof
CSS	Composite scaled sensitivity
PBIAS	Percent Bias
NSE	Nash–Sutcliffe efficiency coefficient
RMSE	Root Mean Square Error

References

1. Shao, M.; Zhao, G.; Kao, S.; Cuo, L.; Rankin, C.; Gao, H. Quantifying the effects of urbanization on floods in a changing environment to promote water security—A case study of two adjacent basins in Texas. *J. Hydrol.* **2020**, *589*, 125154. [CrossRef]
2. Qi, M.; Yang, Y.; Zhang, X.; Zhang, X.; Wang, M.; Zhang, W.; Lu, X.; Tong, Y. Pollution reduction and operating cost analysis of municipal wastewater treatment in China and implication for future wastewater management. *J. Clean. Prod.* **2020**, *253*, 120003. [CrossRef]
3. Müller, A.; Österlund, H.; Marsalek, J.; Viklander, M. The pollution conveyed by urban runoff: A review of sources. *Sci. Total Environ.* **2020**, *709*, 136125. [CrossRef]
4. Huang, L.; Han, X.; Wang, X.; Zhang, Y.; Yang, J.; Feng, A.; Li, J.; Zhu, N. Coupling with high-resolution remote sensing data to evaluate urban non-point source pollution in Tongzhou, China. *Sci. Total Environ.* **2022**, *831*, 154632. [CrossRef]
5. Ma, Y.; Hao, S.; Zhao, H.; Fang, J.; Zhao, J.; Li, X. Pollutant transport analysis and source apportionment of the entire non-point source pollution process in separate sewer systems. *Chemosphere* **2018**, *211*, 557–565. [CrossRef]
6. Lin, B.; An, X.; Zhao, C.; Gao, Y.; Liu, Y.; Qiu, B.; Qi, F.; Sun, D. Analysis of urban composite non-point source pollution characteristics and its contribution to river DOM based on EEMs and FT-ICR MS. *Water Res.* **2024**, *266*, 122406. [CrossRef]
7. Sun, S.; Barraud, S.; Castebrunet, H.; Aubin, J.B.; Marmonier, P. Long-term stormwater quantity and quality analysis using continuous measurements in a French urban catchment. *Water Res.* **2015**, *85*, 432–442. [CrossRef]
8. Fauvel, B.; Cauchie, H.M.; Gantzer, C.; Ogorzaly, L. Contribution of hydrological data to the understanding of the spatio-temporal dynamics of F-specific RNA bacteriophages in river water during rainfall-runoff events. *Water Res.* **2016**, *94*, 328–340. [CrossRef] [PubMed]
9. Novotny, V. Integrating diffuse/nonpoint pollution control and water body restoration into watershed management. *J. Am. Water Resour. Assoc.* **1999**, *35*, 717–727. [CrossRef]
10. Hobbiea, S.E.; Finlaya, J.C.; Jankea, B.D.; Nidzgorskia, D.A.; Milletb, D.B.; Bakerc, L.A. Contrasting nitrogen and phosphorus budgets in urban watersheds and implications for managing urban water pollution. *Proc. Natl. Acad. Sci. USA* **2017**, *114*, E4116. [CrossRef] [PubMed]
11. Liu, Y.; Chen, W.; Li, D.; Huang, Z.; Shen, Y.; Liu, Y. Cyanobacteria-/cyanotoxin-contaminations and eutrophication status before Wuxi Drinking Water Crisis in Lake Taihu, China. *J. Environ. Sci.* **2011**, *23*, 575–581. [CrossRef]
12. Ni, Y. Characteristics and Control Progress for Controlling Urban Non-point Source Pollution. *Environ. Sci. Manag.* **2008**, *33*, 53–57. (In Chinese)
13. Li, W.; Wang, J.; Zhou, Y.; Zhang, P.; Bai, X. Effects of heavy rain on the concentrations and forms of carbon, nitrogen and phosphorus in urban rivers of northern China. *Environ. Sci. Pollut. Res.* **2023**, *30*, 64971–64981. [CrossRef]
14. Zhang, X.; Chen, L.; Yu, Y.; Shen, Z. Water quality variability affected by landscape patterns and the associated temporal observation scales in the rapidly urbanizing watershed. *J. Environ. Manag.* **2021**, *298*, 113523. [CrossRef]
15. Ma, Y.; Wang, S.; Zhang, X.; Shen, Z. Transport process and source contribution of nitrogen in stormwater runoff from urban catchments. *Environ. Pollut.* **2021**, *289*, 117824. [CrossRef]

16. Zhao, L.; Liu, X.; Wang, P.; Hua, Z.; Zhang, Y.; Xue, H. N, P, and COD conveyed by urban runoff: A comparative research between a city and a town in the Taihu Basin, China. *Environ. Sci. Pollut. Res.* **2021**, *28*, 56686–56695. [CrossRef] [PubMed]
17. Huq, E.; Abdul-Aziz, O.I. Climate and land cover change impacts on stormwater runoff in large-scale coastal-urban environments. *Sci. Total Environ.* **2021**, *778*, 146017. [CrossRef] [PubMed]
18. Ross, C.A.; Moslenko, L.L.; Biagi, K.M.; Oswald, C.J.; Wellen, C.C.; Thomas, J.L.; Raby, M.; Sorichetti, R.J. Total and dissolved phosphorus losses from agricultural headwater streams during extreme runoff events. *Sci. Total Environ.* **2022**, *848*, 157736. [CrossRef]
19. Lai, Q.; Ma, J.; He, F.; Wei, G. Response Model for Urban Area Source Pollution and Water Environmental Quality in a River Network Region. *Int. J. Environ. Res. Public Health* **2022**, *19*, 10546. [CrossRef] [PubMed]
20. Ding, F.; Liu, Y.; Wang, L.; Liu, H.; Ji, C.; Zhang, L.; Wu, D. Analysis of the palladium response relationship of a receiving water body under multiple scenario changes in rainfall-runoff pollution. *Environ. Sci. Pollut. Res.* **2021**, *28*, 26684–26696. [CrossRef]
21. Zhao, D.; Wei, T.; Jia, Z.; Feng, J.; Kong, Y.; Li, Y. The influence of rainfall and catchment characteristics on runoff generation in urban catchments-a case study in Hebi City of China. *Environ. Monit. Assess.* **2022**, *194*, 188. [CrossRef] [PubMed]
22. Yun, D.; Kang, D.; Cho, K.H.; Baek, S.S.; Jeon, J. Characterization of micropollutants in urban stormwater using high-resolution monitoring and machine learning. *Water Res.* **2023**, *235*, 119865. [CrossRef] [PubMed]
23. Wang, Y.; Thompson, A.M.; Selbig, W.R. Predictive models of phosphorus concentration and load in stormwater runoff from small urban residential watersheds in fall season. *J. Environ. Manag.* **2022**, *315*, 115171. [CrossRef]
24. Xing, L.; Tao, M.; Zhang, Q.; Kong, M.; Sun, J.; Jia, S.; Liu, C.H. Occurrence, spatial distribution and risk assessment of organophosphate esters in surface water from the lower Yangtze River Basin. *Sci. Total Environ.* **2020**, *734*, 139380. [CrossRef]
25. El-Nakib, S.; Alameddine, I.; Massoud, M.; Abou Najm, M. Nutrient pollutant loading and source apportionment along a Mediterranean river. *Environ. Monit. Assess.* **2020**, *192*, 274. [CrossRef]
26. Meierdiercks, K.L.; Smith, J.A.; Baeck, M.L.; Miller, A.J. Analyses of Urban Drainage Network Structure and its Impact on Hydrologic Response. *J. Am. Water Resour. Assoc.* **2010**, *46*, 932–943. [CrossRef]
27. Cheng, H.; Lin, C.; Wang, L.; Xiong, J.; Peng, L.; Zhu, C. The Influence of Different Forest Characteristics on Non-point Source Pollution: A Case Study at Chaohu Basin, China. *Int. J. Environ. Res. Public Health* **2020**, *17*, 1790. [CrossRef]
28. Song, X.X.; Hou, D.B.; Huang, P.J.; Zhang, G.X. Research on Dynamic Early Warning Technology of Water Pollution Emergency Based on Pollutant Dispersion Simulation. *Appl. Mech. Mater.* **2013**, *316–317*, 682–685. [CrossRef]
29. Chen, L.; Dai, Y.; Zhi, X.; Xie, H.; Shen, Z. Quantifying nonpoint source emissions and their water quality responses in a complex catchment: A case study of a typical urban-rural mixed catchment. *J. Hydrol.* **2018**, *559*, 110–121. [CrossRef]
30. Xue, J.; Wang, Q.; Zhang, M. A review of non-point source water pollution modeling for the urban-rural transitional areas of China: Research status and prospect. *Sci. Total Environ.* **2022**, *826*, 154146. [CrossRef]
31. Zhang, P.; Yang, Y.; Chen, L.; Xie, H.; Shen, Z. Applying copulas to predict the multivariate reduction effect of best management practices. *J. Environ. Manag.* **2020**, *267*, 110641. [CrossRef]
32. Niazi, M.; Nietch, C.; Maghrebi, M.; Jackson, N.; Bennett, B.R.; Tryby, M.; Massoudieh, A. Storm Water Management Model: Performance Review and Gap Analysis. *J. Sustain. Water Built Environ.* **2017**, *3*, 04017002. [CrossRef]
33. Zhang, B.; Chen, M.; Ma, Z.; Zhang, Z.; Yue, S.; Xiao, D.; Zhu, Z.; Wen, Y.; Lu, G. An online participatory system for SWMM-based flood modeling and simulation. *Environ. Sci. Pollut. Res.* **2021**, *29*, 7322–7343. [CrossRef]
34. Hou, X.; Qin, L.; Xue, X.; Xu, S.; Yang, Y.; Liu, X.; Li, M. A city-scale fully controlled system for stormwater management: Consideration of flooding, non-point source pollution and sewer overflow pollution. *J. Hydrol.* **2021**, *603*, 127155. [CrossRef]
35. Danish Hydraulic Institute. *MIKE11-A Modelling System for Rivers and Channels User Guide*; DHI Water & Environment: Hørsholm, Denmark, 2022.
36. Khatooni, K.; Hooshyaripor, F.; MalekMohammadi, B.; Noori, R. A new approach for urban flood risk assessment using coupled SWMM–HEC-RAS-2D model. *J. Environ. Manag.* **2025**, *374*, 123849. [CrossRef]
37. Li, Y.; Badu Osei, F.; Hu, T.; Shi, Y.; Stein, A. Urban inundation mapping by coupling 1D − 2D models and model comparison. *Int. J. Appl. Earth Obs. Geoinf.* **2024**, *130*, 103869. [CrossRef]
38. Jiang, Y.; Li, J.; Gao, J.; Xia, J. A multi-objective optimization and evaluation framework for LID facilities considering urban surface runoff and shallow groundwater regulation. *J. Clean. Prod.* **2024**, *478*, 143921. [CrossRef]
39. Chen, L.; Guo, C.; Yu, Y.; Zhou, X.; Fu, Y.; Wang, S.; Ma, Y.; Shen, Z. Optimization of green infrastructures for sustaining urban stormwater quality and quantity: An integrated resilience evaluation. *J. Hydrol.* **2024**, *640*, 131682. [CrossRef]
40. Fonseca, A.; Botelho, C.; Boaventura, R.A.R.; Vilar, V.J.P. Integrated hydrological and water quality model for river management: A case study on Lena River. *Sci. Total Environ.* **2014**, *485–486*, 474–489. [CrossRef]
41. Imteaz, M.A.; Hossain, I.; Anwar, A.H.M.F. Continuous simulations of nutrients and BOD through a stream section. *Int. J. Water* **2015**, *9*, 144–156. [CrossRef]

42. Lian, H.; Lei, Q.; Zhang, X.; Yen, H.; Wang, H.; Zhai, L.; Liu, H.; Huang, J.-C.; Ren, T.; Zhou, J.; et al. Effects of anthropogenic activities on long-term changes of nitrogen budget in a plain river network region: A case study in the Taihu Basin. *Sci. Total Environ.* **2018**, *645*, 1212–1220. [CrossRef]
43. Qin, B.; Zhu, G.; Gao, G.; Zhang, Y.; Li, W.; Paerl, H.W.; Carmichael, W.W. A drinking water crisis in Lake Taihu, China: Linkage to climatic variability and lake management. *Environ. Manag.* **2010**, *45*, 105–112. [CrossRef]
44. Rossman, L.A. *Storm Water Management Model User's Manual Version 5.1*; EPA/600/R-14/413b; U.S. Environmental Protection Agency: Washington, DC, USA, 2015.
45. Pan, Y.; Guo, J.; Yang, L.; Yuan, Q.; Ren, Z.; Wang, L. Numerical Simulations of Non-Point Source Pollution in a Small Urban Catchment: Identification of Pollution Risk Areas and Effectiveness of Source-Control Measures. *Water* **2021**, *13*, 96. [CrossRef]
46. Feng, L.; Hu, P.; Wang, H.; Chen, M.M.; Han, J. Improving City Water Quality through Pollution Reduction with Urban Floodgate Infrastructure and Design Solutions: A Case Study in Wuxi, China. *Int. J. Environ. Res. Public Health* **2022**, *19*, 10976. [CrossRef]
47. Ji, H.; Peng, D.; Fan, C.; Zhao, K.; Gu, Y.; Liang, Y. Assessing effects of non-point source pollution emission control schemes on Beijing's sub-center with a water environment model. *Urban Clim.* **2022**, *43*, 101148. [CrossRef]
48. Elder, J. The dispersion of marked fluid in turbulent shear flow. *J. Fluid Mech.* **1959**, *5*, 544–560. [CrossRef]
49. Dahlstrom, D.J. Calibration and Uncertainty Analysis for Complex Environmental Models. *Groundwater* **2015**, *53*, 673–674. [CrossRef]
50. Liang, H.; Hu, K.; Li, B. Parameter optimization and sensitivity analysis of soil-crop system model using PEST. *Trans. Chin. Soc. Agric. Eng.* **2016**, *32*, 78–85. (In Chinese) [CrossRef]
51. Bhattarai, A.; Steinbeck, G.; Grant, B.B.; Kalcic, M.; King, K.; Smith, W.; Xu, N.; Deng, J.; Khanal, S. Development of a calibration approach using DNDC and PEST for improving estimates of management impacts on water and nutrient dynamics in an agricultural system. *Environ. Model. Softw.* **2022**, *157*, 105494. [CrossRef]
52. Busico, G.; Colombani, N.; Fronzi, D.; Pellegrini, M.; Tazioli, A.; Mastrocicco, M. Evaluating SWAT model performance, considering different soils data input, to quantify actual and future runoff susceptibility in a highly urbanized basin. *J. Environ. Manag.* **2020**, *266*, 110625. [CrossRef] [PubMed]
53. Feng, L.; Li, Q.; Zhang, L.; Wang, H.; Wang, W.; Han, J.; Li, B.-l. Exploring the effect of floodgates operation systems on water environmental capacity in a regulated river network of Wuxi, China. *J. Clean. Prod.* **2021**, *299*, 126743. [CrossRef]
54. Tang, S.; Song, Y.; Wang, Y.; Jia, Z.; Gao, X.; Cheng, N.; Lu, T. Optimizing stormwater runoff treatment: The role of two-stage tandem rain gardens. *Environ. Res.* **2024**, *262*, 119831. [CrossRef]
55. Morihama, A.C.; Amaro, C.; Tominaga, E.N.; Yazaki, L.F.; Pereira, M.C.; Porto, M.F.; Mukai, P.; Lucci, R.M. Integrated solutions for urban runoff pollution control in Brazilian metropolitan regions. *Water Sci. Technol.* **2012**, *66*, 704–711. [CrossRef]
56. Guo, J.; Pan, Y.; Chen, R.; He, S.; Qi, W.; Yang, H.; Wang, L. Tracing nitrogen and phosphorus pollution in urban runoff: Insights from isotopic tracers and SWMM modeling. *J. Clean. Prod.* **2024**, *472*, 143513. [CrossRef]
57. Xiong, Q.; Song, Y.; Shen, J.; Liu, C.; Chai, Y.; Wang, S.; Wu, X.; Cheng, C.; Wu, J. Fluorescence fingerprint as an indicator to identify urban non-point sources in urban river during rainfall period. *Environ. Res.* **2024**, *245*, 118009. [CrossRef]
58. Li, X.; Yang, S.; Li, J.; Li, Y.; Liu, D.; Xiong, F.; Li, J. Impacts of rainfall characteristics and land cover types on an urban river water quality: A case study of sponge city Beijing. *J. Clean. Prod.* **2025**, *505*, 145411. [CrossRef]
59. Yang, S.; Yang, G.; Li, B.; Wan, R. Water quality improves with increased spatially surface hydrological connectivity in plain river network areas. *J. Environ. Manag.* **2025**, *377*, 124703. [CrossRef] [PubMed]
60. Yu, Z.; Wang, Q.; Xu, Y.; Lu, M.; Lin, Z.; Gao, B. Dynamic impacts of changes in river structure and connectivity on water quality under urbanization in the Yangtze River Delta plain. *Ecol. Indic.* **2022**, *135*, 108582. [CrossRef]
61. Gong, Y.; Yin, D.; Li, J.; Zhang, X.; Wang, W.; Fang, X.; Shi, H.; Wang, Q. Performance assessment of extensive green roof runoff flow and quality control capacity based on pilot experiments. *Sci. Total Environ.* **2019**, *687*, 505–515. [CrossRef] [PubMed]
62. Yang, L.; Li, J.; Zhou, K.; Feng, P.; Dong, L. The effects of surface pollution on urban river water quality under rainfall events in Wuqing district, Tianjin, China. *J. Clean. Prod.* **2021**, *293*, 126136. [CrossRef]
63. Chowdhury, A.; Egodawatta, P.; McGree, J. Pattern-based assessment of the influence of rainfall characteristics on urban stormwater quality. *Water Sci. Technol.* **2023**, *87*, 2292–2303. [CrossRef]
64. Liu, A.; Goonetilleke, A.; Egodawatta, P. Taxonomy for rainfall events based on pollutant wash-off potential in urban areas. *Ecol. Eng.* **2012**, *47*, 110–114. [CrossRef]
65. Wang, X.; Wu, R.; He, Y. Field evidences of fluorescent dissolved organic matter (FDOM) as potential fingerprints for agricultural and urban sources in river environment. *Environ. Sci. Pollut. Res.* **2023**, *30*, 70722–70730. [CrossRef]
66. Yuan, K.; Wan, Q.; Chai, B.; Lei, X.; Kang, A.; Chen, J.; Chen, X.; Shi, H.; He, L.; Li, M. Characterizing the effects of stormwater runoff on dissolved organic matter in an urban river (Jiujiang, Jiangxi province, China) using spectral analysis. *Environ. Sci. Pollut. Res.* **2023**, *30*, 50649–50660. [CrossRef] [PubMed]

67. Zhang, W.; Li, T. The Influence of Objective Function and Acceptability Threshold on Uncertainty Assessment of an Urban Drainage Hydraulic Model with Generalized Likelihood Uncertainty Estimation Methodology. *Water Resour. Manag.* **2015**, *29*, 2059–2072. [CrossRef]
68. Li, N.; McLaughlin, D.; Kinzelbach, W.; Li, W.; Dong, X. Using an ensemble smoother to evaluate parameter uncertainty of an integrated hydrological model of Yanqi basin. *J. Hydrol.* **2015**, *529*, 146–158. [CrossRef]
69. Sharifan, R.A.; Roshan, A.; Aflatoni, M.; Jahedi, A.; Zolghadr, M. Uncertainty and Sensitivity Analysis of SWMM Model in Computation of Manhole Water Depth and Subcatchment Peak Flood. *Procedia—Soc. Behav. Sci.* **2010**, *2*, 7739–7740. [CrossRef]
70. Jiang, Y.; Li, J.; Xia, J.; Gao, J. Sensitivity identification of SWMM parameters and response patterns of runoff pollution on hydrological and water quality parameters. *Ecohydrol. Hydrobiol.* **2025**, *25*, 511–522. [CrossRef]
71. Moriasi, D.; Arnold, J.; Van Liew, M.; Bingner, R.; Harmel, R.D.; Veith, T. Model Evaluation Guidelines for Systematic Quantification of Accuracy in Watershed Simulations. *Trans. ASABE* **2007**, *50*, 885–900. [CrossRef]
72. Gupta, H.V.; Kling, H.; Yilmaz, K.K.; Martinez, G.F. Decomposition of the mean squared error and NSE performance criteria: Implications for improving hydrological modelling. *J. Hydrol.* **2009**, *377*, 80–91. [CrossRef]
73. Chow, M.F.; Yusop, Z.; Abustan, I. Relationship between sediment build-up characteristics and antecedent dry days on different urban road surfaces in Malaysia. *Urban Water J.* **2015**, *12*, 240–247. [CrossRef]
74. Yao, L.; Wu, Z.; Wang, Y.; Sun, S.; Wei, W.; Xu, Y. Does the spatial location of green roofs affects runoff mitigation in small urbanized catchments? *J. Environ. Manag.* **2020**, *268*, 110707. [CrossRef] [PubMed]

Disclaimer/Publisher's Note: The statements, opinions and data contained in all publications are solely those of the individual author(s) and contributor(s) and not of MDPI and/or the editor(s). MDPI and/or the editor(s) disclaim responsibility for any injury to people or property resulting from any ideas, methods, instructions or products referred to in the content.